energies

MDPI

Article

Coordinated Control of Multi-Port Power Router Based on DC Bus Voltage Droop Regulation

Caihong Zhao [1,*], Guanglin Sha [1], Haoqing Wang [1], Pingkang Zheng [2], Ning Liu [1] and Qing Duan [1]

[1] China Electric Power Research Institute Co., Ltd., Beijing 100080, China; wanghaoqing@epri.sgcc.com.cn (H.W.); liuning1@epri.sgcc.com.cn (N.L.)
[2] School of Electrical and Electronic Engineering, Huazhong University of Science and Technology, Wuhan 430074, China
* Correspondence: zhaocaihong@epri.sgcc.com.cn

Abstract: Coordinated operation among various converters within a power router (PR) is crucial for ensuring its normal operation. Since the power balance among converters in a DC PR is reflected by the DC bus voltage level, maintaining stable DC bus voltage control is particularly important as it directly affects the coordinated operation of each converter. This study proposes a coordinated control strategy for multi-port power routers based on DC bus voltage droop regulation, addressing the limitations of existing methods that rely on communication and complex control units. Based on DC bus voltage signals, all power ports automatically switch their operating states, ensuring that only one converter operates in voltage source mode at any given time, thereby maintaining the system's bus voltage and power balance. This enables effective coordination among converters and ensures stable system operation without requiring communication between converters, simplifying control while maintaining internal system stability.

Keywords: power router; DC bus voltage; coordinated control; smooth switching

check for updates

Academic Editor: José Matas

Received: 3 December 2024
Revised: 23 January 2025
Accepted: 11 February 2025
Published: 3 March 2025

Citation: Zhao, C.; Sha, G.; Wang, H.; Zheng, P.; Liu, N.; Duan, Q. Coordinated Control of Multi-Port Power Router Based on DC Bus Voltage Droop Regulation. *Energies* **2025**, *18*, 1243. https://doi.org/10.3390/en18051243

Copyright: © 2025 by the authors. Licensee MDPI, Basel, Switzerland. This article is an open access article distributed under the terms and conditions of the Creative Commons Attribution (CC BY) license (https://creativecommons.org/licenses/by/4.0/).

1. Introduction

A power router (PR) is a highly integrated power electronic conversion device that combines information flow and power flow. It features universality, openness, and compatibility, and is capable of managing, dispatching, and distributing energy at various scales, from household to industrial park to power grid levels. It simultaneously meets the demands of local energy consumption, grid connection, and sharing requirements, achieving a comprehensive utilization of "source-grid-load-storage" integration [1–4].

In a DC power router, the DC bus voltage is influenced by multiple factors, including power fluctuations from renewable energy sources due to environmental factors, variations in load demands, and grid power constraints. Since DC bus voltage stability represents power balance, maintaining stable DC bus voltage control is particularly crucial as it directly affects the coordinated operation of various converters. Recent studies have focused on addressing DC bus voltage control issues. For example, Reference [5] proposes a distributed hierarchical coordination control strategy for photovoltaic storage DC microgrids, designing droop control characteristics for both photovoltaic and energy storage systems to achieve stable operation across various application scenarios. References [6–8] employs a voltage-segmented droop control method to achieve real-time tracking of load changes in energy storage systems in DC microgrids while maintaining an essentially constant bus voltage. Additionally, Reference [9] proposes a comprehensive control technology based on energy

balance for multi-stage conversion power routers, while Reference [10] presents a droop phase shift coordination control strategy for three-port DC power routers.

In recent years, with the rapid development of distributed energy resources and DC microgrids, coordinated control strategies for power routers have attracted significant attention. Reference [11] proposes a control method based on the virtual synchronous generator (VSG) to improve the dynamic performance and stability of power routers. Reference [12] investigates power distribution strategies for multi-port DC power routers based on droop control, optimizing power flow among different ports. Additionally, Reference [13] explores seamless switching control strategies for photo-voltaic energy storage systems, providing new insights into the grid-connected/islanding operation of PRs.

Despite significant theoretical and experimental progress in these studies, most methods still rely on complex communication mechanisms and central controllers, making them difficult to implement in practical applications [14–16]. Therefore, this study proposes a simplified coordinated control strategy that automatically switches operating modes based on DC bus voltage variations, eliminating the need for additional communication mechanisms and significantly enhancing system adaptability and reliability.

This paper focuses on residential application requirements, designing a multi-port PR system with a common DC bus, and investigating the coordinated control of various conversion units within the PR. The common DC bus voltage is divided into three levels, and under grid-connected/islanded and various operating conditions, each port conversion unit autonomously switches its operating mode based on the bus voltage. This achieves smooth transitions between layers, enabling effective coordination among PR conversion units and ensuring stable system operation without requiring communication between converters. While simplifying control, it maintains stable internal system operation. A simulation model was built using Simulink, and an experimental platform was constructed to conduct simulations and experiments under different operating conditions, verifying the effectiveness of the proposed method.

2. PR Composition Architecture and Operating Modes

2.1. PR System Architecture

The current China national standard GB/T 40097-2021 [17] "Energy Router Function Specifications and Technical Requirements" clearly defines the basic functions of power routing: "with electrical energy as the primary control object, it must have three or more power ports, possess the capability for power conversion, transmission, and routing between different electrical parameters, coordinate with upper-level systems, and control and manage connected power sources, energy storage, and loads".

This paper focuses on residential community or household applications, constructing a PR system device with a common DC bus using multi-port converter units. As shown in Figure 1, this PR includes four power unit ports: Port 1 is a bidirectional AC/DC converter, enabling bidirectional power interaction between the PR and the power grid. Port 2 is a unidirectional DC/DC step-down converter, utilizing a Buck circuit in this paper, converting the 750 V DC bus voltage to 220 V DC for DC load use. Port 3 is a unidirectional DC/DC step-up converter, boosting the low-voltage DC output from photovoltaic arrays to the DC bus while controlling the power output of the photovoltaic unit during operation. Port 4 is an energy storage unit, comprising a bidirectional DC/DC converter and storage batteries, used for storing and releasing energy during operation.

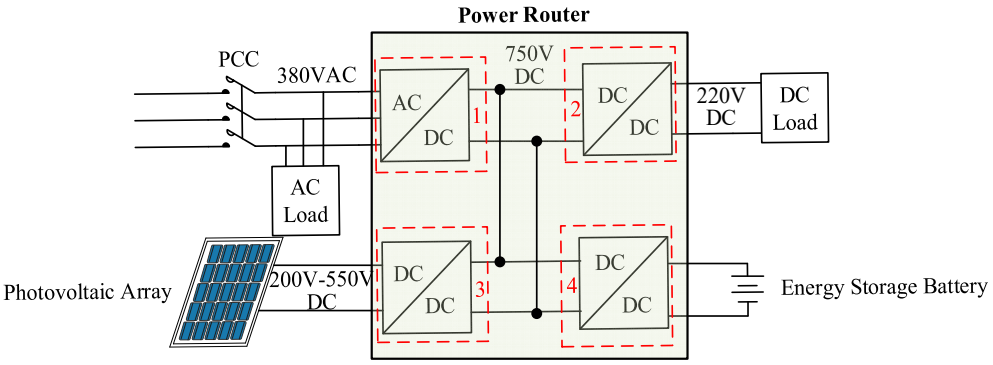


Figure 1. Four-port PR architecture.

2.2. PR Typical Operating Modes

The grid-connected inverter in the PR connects with the public power grid. Under normal operating conditions, the inverter and grid can serve as ideal power balance points: when the system power is insufficient, the grid supplies power to the system's DC bus through the inverter; when the system has surplus power, the DC bus feeds energy back to the grid through the inverter. Therefore, the grid-connected inverter is the DC voltage control terminal, which can maintain a constant PR DC bus voltage. Additionally, current limiting segments are typically set into the inverter control loop to ensure that the converter automatically enters current-limiting mode when the bidirectional power becomes excessive. In Figure 2, ΔU_{dc} indicates the maximum allowable voltage variation for the corresponding converter.

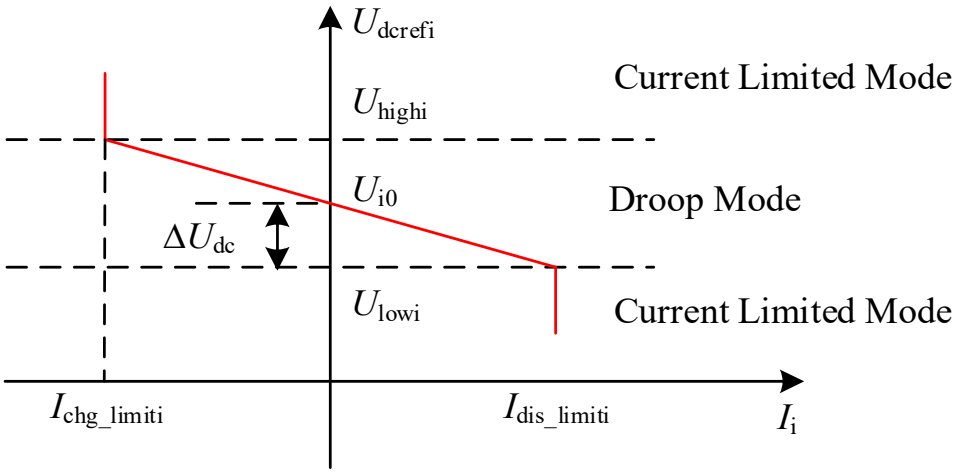


Figure 2. Composite droop control.

When multiple power units such as energy storage, loads, and photovoltaic systems work in conjunction with the inverter, system power coordination and balance employ droop control to coordinate the operating states of various converters according to their output capabilities, while avoiding current surges during converter operating state transitions.

Specifically, this paper classifies PR operating modes into the following three categories:

(1) Free Grid-Connected Mode

When the PR is normally connected to the power grid and the grid energy supply is unrestricted, the PR's grid-connected inverter operates as a voltage source, becoming the system's power balance point to stabilize the DC bus voltage, while the other units operate as current sources. In this mode, the photovoltaic unit always operates in MPPT mode to supply energy to the system, while the energy storage unit charges/discharges the battery according to its SOC.

(2) Current-Limited Grid-Connected Mode

The operation of PR power ports is controlled by coordination controller dispatch commands. When grid-connected inverter power is limited, the power absorbed from or fed to the grid by the grid-connected unit becomes fixed, causing the grid-connected unit to lose its power balancing function and become unable to maintain a constant DC bus voltage. Additionally, when PR participates in energy management dispatch, situations may arise where the grid-connected unit's power is limited, during which the grid-connected inverter cannot control the DC bus voltage constancy. Both these conditions cause the system to enter current-limited grid-connected mode. In this mode, the energy storage unit transitions from the charging state or standby state to voltage source mode operation, controlling DC bus voltage stability and maintaining system power balance.

When the energy storage battery's SOC is within the upper and lower threshold range, the battery can operate normally. When the energy storage unit's output is within the limited power range, the energy storage unit can maintain a stable DC bus voltage within the power router during current-limited grid-connected mode.

(3) PV Power Curtailment Operating Mode

When weather conditions such as light intensity and temperature are favorable, photovoltaic units' output power is high. If the energy storage SOC has reached its upper limit or the energy storage unit's charging power has reached its limit, and the grid-connected unit power has also reached its limit, there will be surplus photovoltaic power, and this power imbalance will cause DC bus voltage to rise. To ensure system safety and stability, the photovoltaic unit needs to exit MPPT mode and operate in power curtailment mode. At this time, the system bus voltage is relatively high, and the photovoltaic converter switches from MPPT mode to constant voltage operation, maintaining a stable system DC bus voltage.

3. DC Bus Voltage-Based Hierarchical Control

Based on the aforementioned three operating modes, this paper adopts the voltage hierarchical control method shown in Figure 3, dividing the system into three layers according to DC bus voltage variations. v_{t1} and v_{t2} are the threshold voltages at switching points in the hierarchical control. Near the switching threshold voltages, voltage hysteresis is employed to prevent frequent switching between different modes, with v_{t1} and v_{t2} selected as 0.02 and 0.05 (per unit values), respectively. S = 1, 2, 3 indicates that the power router is operating in the first, second, or third layer of control, respectively.

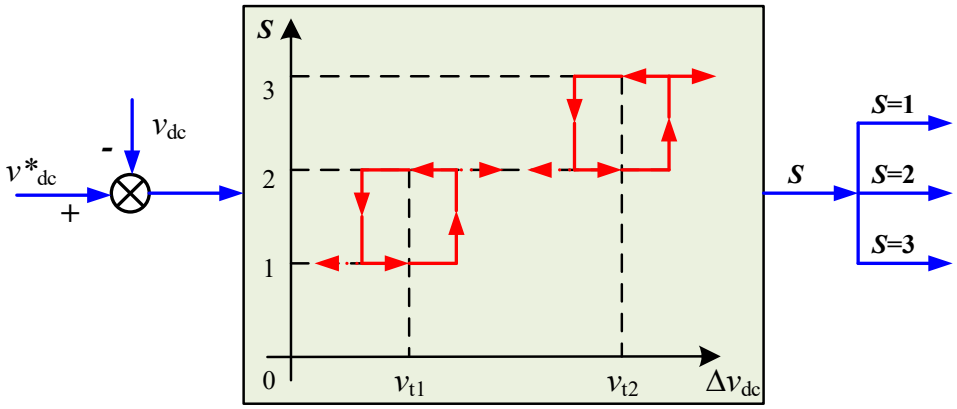
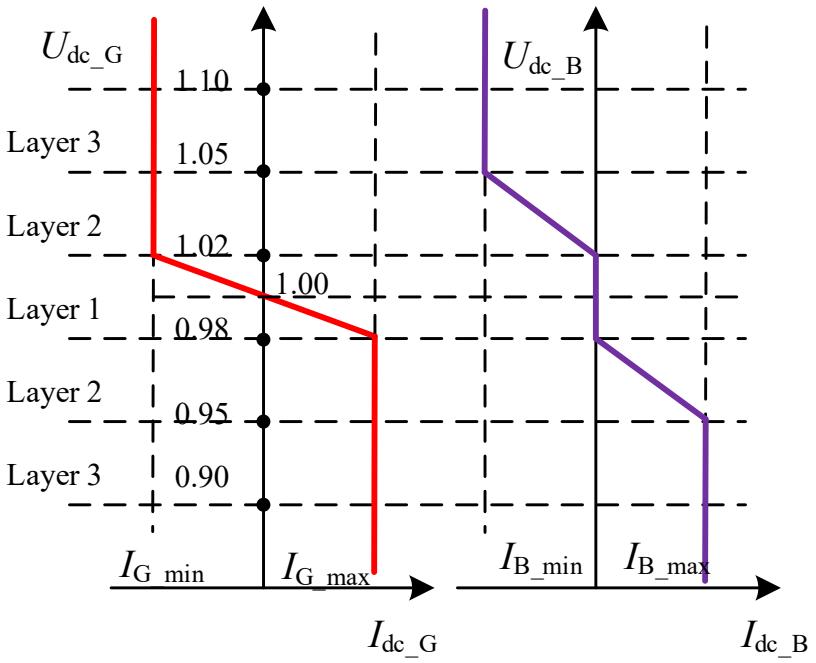


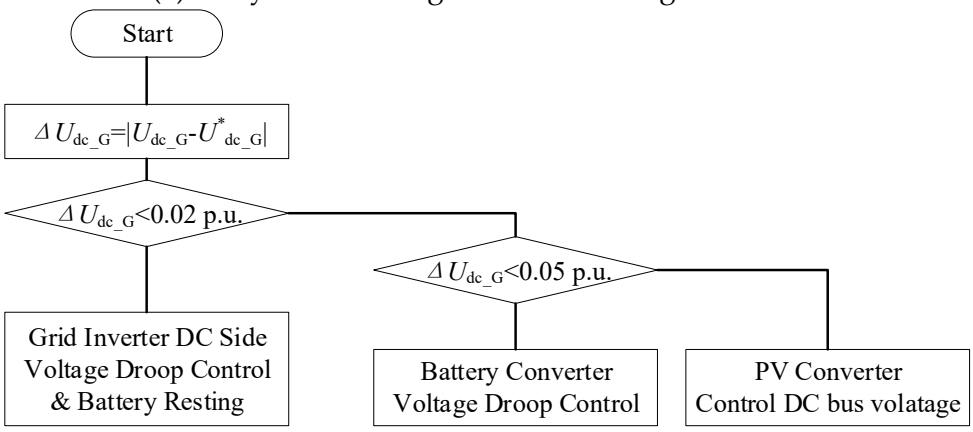
Figure 3. Voltage layered control method for energy routers.

Figure 4 shows a diagram of the voltage hierarchical droop control characteristic adopted in this paper, where U_{dc_G} and U_{dc_B} represent the power source external charac-

teristics of the grid-connected unit inverter and energy storage unit bidirectional energy storage converter in different layers, respectively. In the figure, the horizontal axis represents the converter output current, while the vertical axis represents DC bus voltage variations, with the voltage variations shown in per-unit values. In the diagram, a positive current direction indicates that the grid-connected unit inverter and energy storage unit bidirectional energy storage converter are supplying power to the PR DC bus, while a negative current direction indicates they are absorbing power from the DC bus.



(**a**) 3 Layers according to DC bus voltage variation.



(**b**) Flowchart of control mode switching.

Figure 4. Voltage layered droop control characteristic diagram.

3.1. First Layer—Grid-Dominated Control Layer

When the DC bus voltage variation is within ±2%, the PR operates in the first layer, namely the grid-dominated control layer, corresponding to the PR's free grid-connected mode. In this layer of control, the grid plays a dominant role, with the system DC bus voltage being controlled by the inverter operating in rectification mode, while the inverter simultaneously handles system power balance tasks. The energy storage unit is then charged, storing electrical energy in batteries for backup, while the photovoltaic unit operates in MPPT mode to capture solar energy, integrating clean solar power into the ER.

The grid-connected inverter's control loop employs DC voltage control in the outer loop, operating as a voltage source to ensure DC-side voltage stability, while using current control in the inner loop. Additionally, to enable switching between different layers, voltage droop control is superimposed on the voltage loop. Figure 4 shows the inverter U-I droop characteristic curve in the first layer control.

$$U_{dc_G} = U^*_{dc_G} - k_G I_{dc_G} \quad (1)$$

In this equation, k_G is the inverter droop coefficient, where $k_G = 0.02/I_{G_max}$, where I_{G_max} represents the maximum DC-side current of the inverter; $U^*_{dc_G}$ is the voltage reference value in the first layer control. In this paper's first layer control $U^*_{dc_G} = 750$ V. The inverter's control loop at this time is shown in Figure 5.

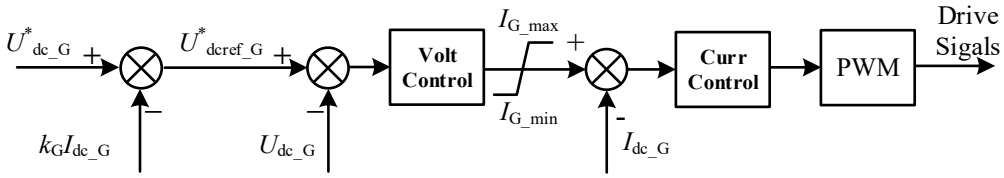


Figure 5. Control loop of inverter.

The battery in the energy storage unit is in a charging state. Figure 6 shows a control block diagram for battery charging, which employs constant current charging. Both over-charging and over-discharging shorten the battery's life, so the battery SOC needs to be controlled within a certain range. This paper limits the SOC range to 20%~80%, meaning the battery charging SOC upper limit is 80% and the discharging SOC lower limit is 20%. During battery charging, the battery energy management system issues charging current commands and battery SOC values. Based on the battery SOC value, PWM signals undergo logical control before outputting corresponding drive signals, with PWM signals blocked to stop charging when the SOC exceeds 80%.

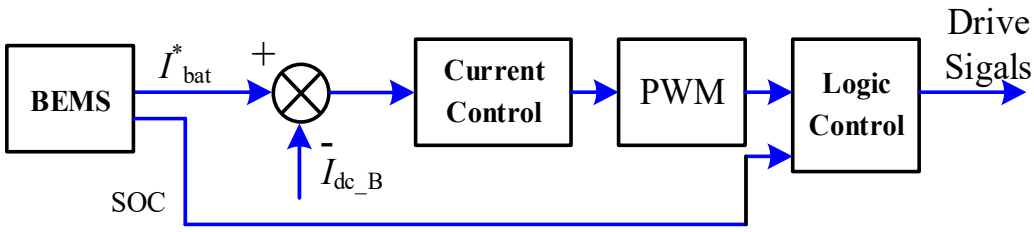


Figure 6. Block diagram of battery charging current loop control (BEMS—battery energy management system).

The photovoltaic converter in the photovoltaic unit operates in MPPT mode, maximizing the conversion of solar energy into electrical energy for input to the system DC bus. The load unit employs dual-loop control with a voltage outer loop and a current inner loop to provide stable DC power to DC loads.

3.2. Second Layer—Energy Storage-Dominated Control Layer

When the DC bus voltage variation is within $2\% < \Delta U_{dc} < 5\%$, the PR operates in the second layer, namely the energy storage-dominant control layer. This corresponds to the grid-connected current limiting mode of the PR. In this mode, the inverter in the grid-connected unit reaches the limit of current output or absorption, losing the ability to maintain a constant bus voltage. In this layer of control, the photovoltaic unit still operates in the MPPT mode, absorbing solar energy, while the voltage of the DC bus is controlled by the energy storage unit.

At this time, the bidirectional energy storage converter in the energy storage unit switches from current source mode to voltage source mode to stabilize the voltage on the DC bus side. According to the droop control characteristics of the energy storage converter shown in Figure 4, the U-I droop characteristic curve of the energy storage converter can be expressed as follows:

$$U_{dc_B} = U^*_{dc_B} - k_B I_{dc_B} \quad (2)$$

In the equation, $k_B = 0.03/I_{B_max}$ is the droop coefficient of the bidirectional energy storage converter, and I_{B_max} is the maximum current on the DC side of the bidirectional energy storage converter. Based on the characteristics of droop control discussed earlier, to increase the energy storage capacity of the system, when there are multiple sets of energy storage batteries in the system, the droop coefficient for each set of energy storage units can be designed according to the power distribution of different energy storage units. This allows for more precise control of the DC bus voltage. $U^*_{dc_B}$ is the voltage reference value in the second layer of control, which can be $U^*_{dc_B} = 1.02$ p.u. or $U^*_{dc_B} = 0.98$ p.u.

The control loop of the energy storage converter in this layer is shown in Figure 7. In this layer of control, the outer loop of the energy storage converter uses a voltage loop with droop characteristics. The output of the droop control serves as the setpoint for the voltage controller, and the output of the voltage loop serves as the command for battery charging and discharging. After passing through the current controller, it generates a PWM signal to control the operation of the bidirectional energy storage converter.

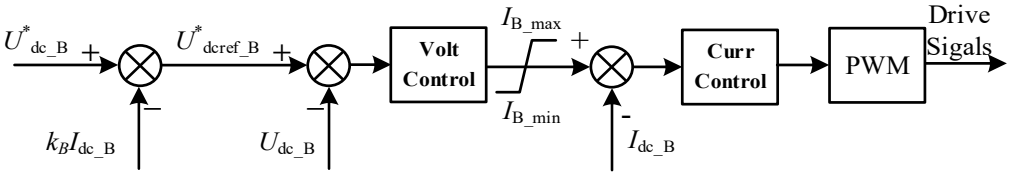


Figure 7. Control loop of bidirectional converter.

3.3. Third Layer—Photovoltaic-Dominated Control Layer

When the DC bus voltage variation is $\Delta U_{dc} > 5\%$, the PR operates in the third layer, namely the photovoltaic-dominated control layer, corresponding to the power curtailment operating mode. At this time, the energy storage unit's battery SOC has reached the system-specified upper limit, or the energy storage unit is charging the battery at maximum charging current, while the photovoltaic power is relatively high. According to previous derivations, the bus voltage will continuously rise at this time. To ensure system bus voltage stability, the photovoltaic unit needs to exit MPPT mode and switch to constant voltage operation mode.

The control loop for the photovoltaic converter power curtailment operation is shown in Figure 8. ΔV_{PV} is added to the traditional MPPT control output VMPPT. At this time, due to the high photovoltaic power and low system power consumption, bus power imbalance leads to an increase in voltage; namely, $V_{dc} > V_{dcref}$ occurs, requiring a reduction in photovoltaic power. The difference between the DC bus voltage V_{dc} and the photovoltaic unit constant voltage reference value V_{dcref} is processed through a PI controller and superimposed with MPPT control output. At this time, the PI controller output is positive, which will control the photovoltaic array to work in the downward slope region, reducing the photovoltaic output power and controlling the system DC bus voltage at the V_{dcref} value. In the third layer control, V_{dcref} is set to 1.075 pu.

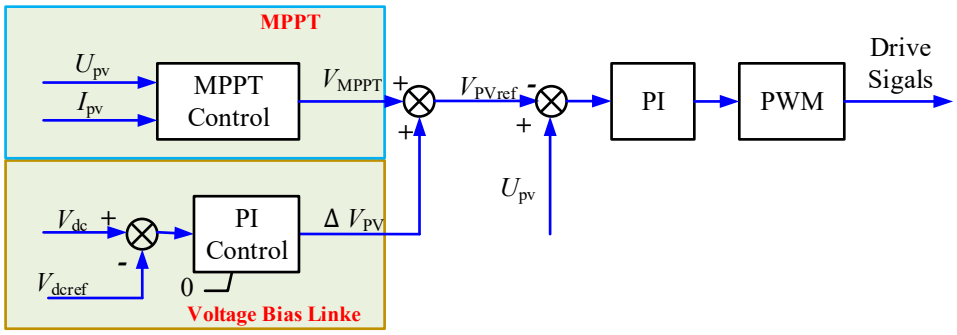


Figure 8. Control block diagram of photovoltaic converter.

4. Hierarchical Control Simulation Analysis of Power Router

4.1. Simulation System Description

To verify the effectiveness of the hierarchical coordinated control adopted in this PR, a simulation model was built in Simulink, as shown in Figure 9.

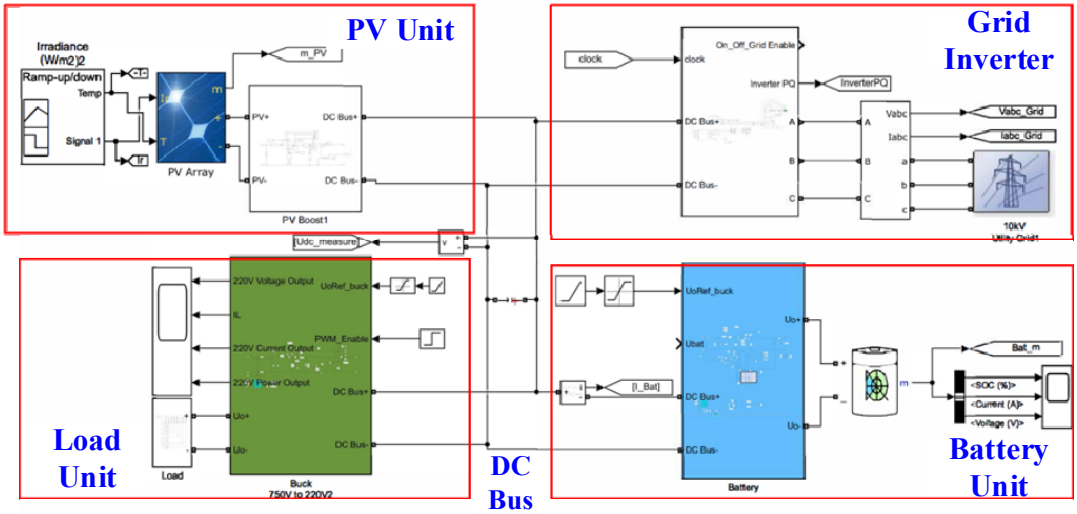


Figure 9. System simulation diagram. Photovoltaic unit.

In this simulation, the system DC bus voltage is 750 V; the DC load-rated voltage is 220 V, using resistive loads to simulate load conditions. Table 1 shows the detailed simulation parameters used.

Table 1. Simulation parameters.

DC Bus Voltage Value	Rated voltage 750 V
Photovoltaic Unit	Maximum power 12 kW
Energy Storage Unit	Bidirectional energy storage converter rated power 10 kW Storage battery: Lithium battery, rated voltage 330 V, rated capacity 10 Ah
Grid-Connected Unit	Rated power 7.5 kW
Load Unit	Rated voltage 220 V, maximum power 10 kW

4.2. Free Grid-Connected Mode Simulation Analysis

Table 2 shows the simulation time node settings for the free grid-connected mode.

At the start of the simulation, the grid-connected unit inverter starts and establishes a DC bus voltage of 750 V. At t_1 = 0.5 s, the energy storage unit starts, with a battery SOC at

79.96%, below 80%. The bidirectional energy storage converter begins charging the battery with a charging power of approximately 4 kW, and the battery SOC gradually increases. As shown in Figure 10a, the DC bus voltage decreases from 750 V to 742 V under droop control. At t_2 = 1 s, the DC load unit starts with no load, establishing an output voltage of 220 V, with the bus voltage remaining essentially constant. At t_3 = 1.5 s, the DC load unit suddenly increases the load to 0.5 kW, causing the DC bus voltage to slightly decrease and the battery charging power to reduce.

Table 2. Simulation time node settings for the system in free networking mode.

Simulation Time T/S	Simulation Settings
0	Start simulation, grid-connected inverter establishes DC bus voltage 750 V
0.5(T1)	Energy storage unit starts, charges storage battery
1(T2)	DC load unit converter starts with no load, establishes 220 V voltage
1.5(T3)	DC load unit loads 0.5 kW
2(T4)	Photovoltaic unit starts MPPT control
3(T5)	Light intensity increases
3.2(T6)	Light intensity reaches maximum value and remains constant
4(T7)	Light intensity suddenly drops
4.5(T8)	DC load unit loads 1 kW
5(T9)	Light intensity increases, restores to maximum value
5.5(T10)	DC load unit loads 0.5 kW
6	Simulation ends

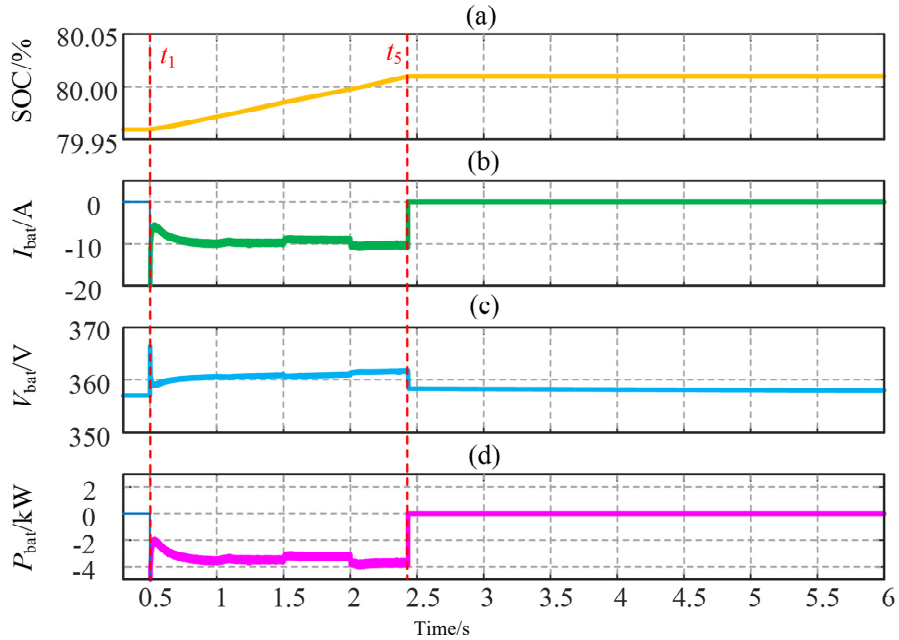


Figure 10. Free grid-connected mode energy storage unit output waveforms: (**a**) battery SOC; (**b**) battery current; (**c**) battery voltage; (**d**) battery power.

At t_4 = 2 s, the photovoltaic unit initiates MPPT control, beginning to convert solar energy into electrical energy for system DC bus input, causing the bus voltage to rise and the battery charging power to increase. At t_5 = 2.435 s, the battery SOC reaches 80%, the energy storage unit shuts down, stops battery charging, and the energy storage unit power reduces to 0. At t_6 = 3 s, the environmental light intensity increases from an initial 100 W/m² to 500 W/m², the photovoltaic power gradually increases to 6 kW, and the bus voltage rises to 760 V (Figure 10). At t_7 = 3.2 s, the light intensity reaches its maximum and remains constant, the bus voltage stabilizes around 760 V, and the inverter's grid-connected power

increases. At t_8 = 4 s, due to certain reasons, the environmental light intensity suddenly drops to 300 W/m², causing the photovoltaic current and power to decrease to 3.5 kW. Affected by photovoltaic output fluctuation, the bus voltage and inverter power feedback to the grid decrease. At t_9 = 4.5 s, the load unit is 1 kW, the photovoltaic power remains unchanged, and the grid-connected unit inverter power decreases to 2 kW. At t_{10} = 5 s, the environmental light intensity recovers, the photovoltaic output restores to 6 kW, the load power consumption remains unchanged, the bus voltage rises, and the grid-connected power increases to 4.5 kW. At t_{11} = 5.5 s, the load unit suddenly adds another 0.5 kW load, and the grid-connected power reduces to 4 kW.

As shown in Figure 11, throughout the system's entire variation process, the bus voltage changes remain within ±2%. While the photovoltaic output continuously fluctuates and the load unit power constantly changes, the grid-connected unit inverter adjusts the energy exchange between the energy router and power grid according to droop control, maintaining the system bus voltage within a relatively constant range. When the battery SOC reaches 80%, charging stops to prevent overcharging.

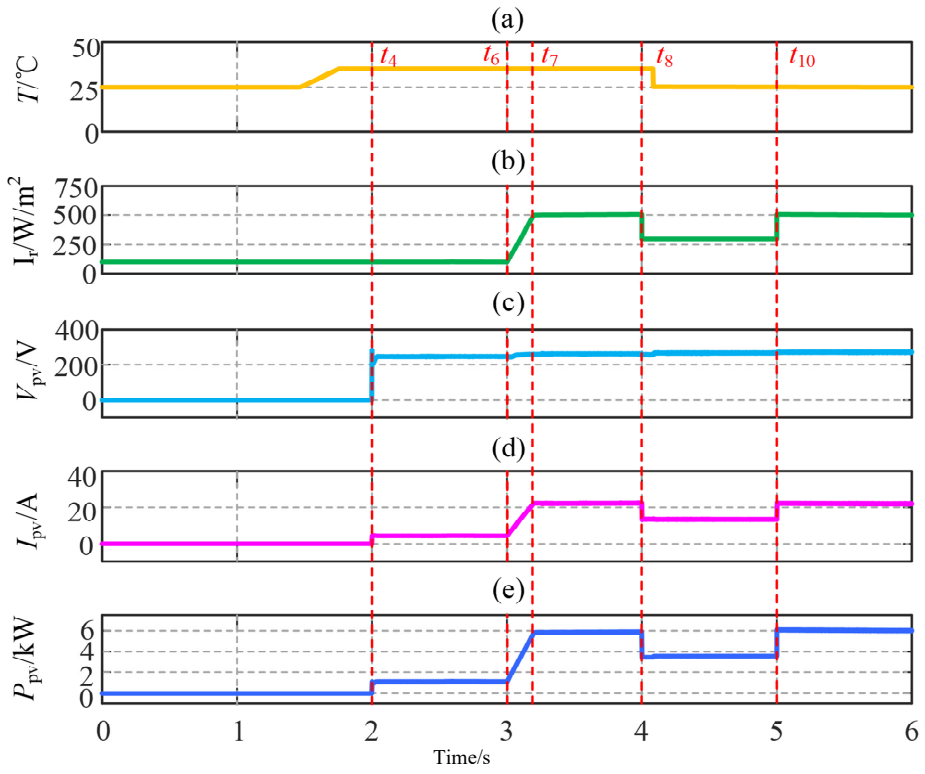


Figure 11. Free grid-connected mode photovoltaic unit output waveforms: (**a**) ambient temperature; (**b**) light intensity; (**c**) photovoltaic voltage; (**d**) photovoltaic current; (**e**) photovoltaic power.

4.3. Current-Limited Grid-Connected Mode Simulation Analysis

At the start of the simulation, the grid-connected unit inverter starts and establishes a DC bus voltage of 750 V (Table 3). At t_1 = 0.5 s, the energy storage unit starts with a battery SOC at 78%, below 80%. The bidirectional energy storage converter begins charging the battery, and the battery SOC gradually increases. As shown in Figure 12a, the DC bus voltage decreases from 750 V to 742 V under droop control. At t_2 = 1 s, the DC load unit starts with a 5 kW load, and the bus voltage decreases, simulating the system receiving a power limitation dispatch command. At this time, the maximum power that the grid-connected unit can absorb from the grid is 5 kW, so the battery charging power drops to 0, and the grid-connected unit absorbs 5 kW from the grid. At 1.088 s, the grid-connected unit inverter power reaches the power limit value of 5 kW, the bus voltage is 731 V, the system

bus voltage enters the second layer, the energy storage converter begins to dominate the system bus voltage stability control, and the battery SOC starts to decrease, as shown in Figure 12a.

Table 3. Simulation time node settings for current-limited grid-connected mode.

Simulation Time T/S	Simulation Settings
0	Start simulation, grid-connected inverter establishes DC bus voltage 750 V
0.5(T1)	Energy storage unit starts, charges storage battery
1(T2)	DC load unit converter starts with 5 kW load
1.5(T3)	DC load unit loads 1.25 kW
2(T4)	Photovoltaic unit starts MPPT control, light intensity relatively low
2.5(T5)	DC load unit loads 1.25 kW
3(T6)	DC load unit loads 1.25 kW
4(T7)	DC load unit loads 2.5 kW
5(T8)	Light intensity increases
5.5(T9)	Light intensity reaches maximum value and remains constant
6(T10)	DC load unit reduces load by 2.5 kW
7(T11)	DC load unit reduces load by 3.75 kW, switches to no load
8	Simulation ends

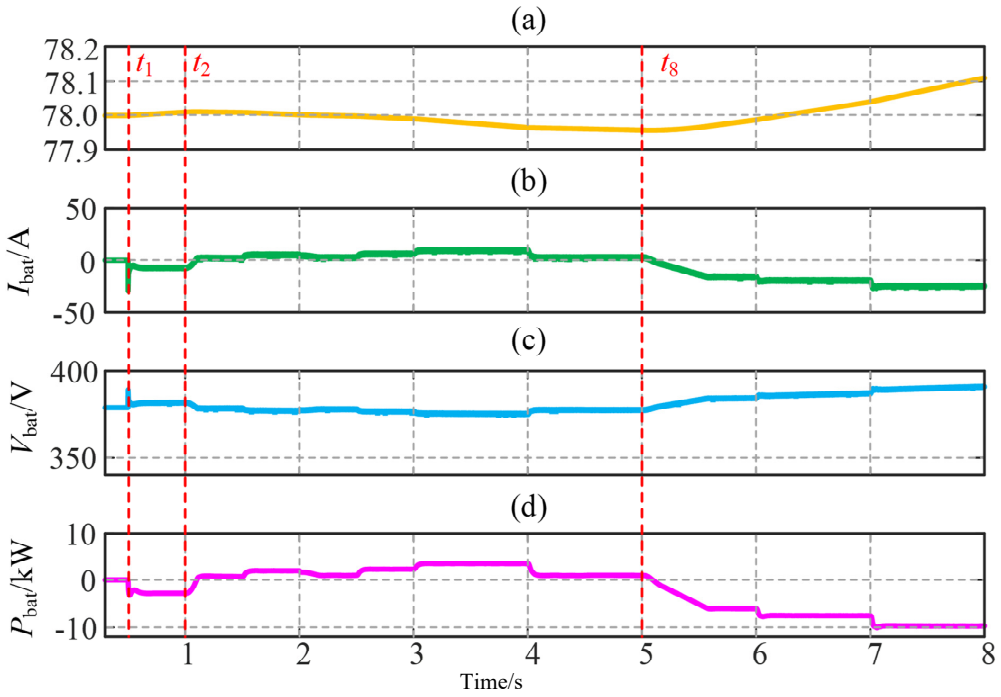


Figure 12. Current-limited grid-connected mode energy storage unit output waveforms: (**a**) battery SOC; (**b**) battery current; (**c**) battery voltage; (**d**) battery power.

At t_3 = 1.5 s, the DC load increases by 1.25 kW. Due to power limitation on the grid-connected unit inverter, power absorbed from the grid is insufficient to meet the load power demand. At this time, the power deficit is supplied by the energy storage unit. As shown in Figure 13e, the energy storage unit begins to input power to the DC bus. At t_4 = 2 s, the photovoltaic unit begins operation with a relatively low light intensity of only 100 W/m², resulting in a photovoltaic output of only around 1.1 kW. The operation of the photovoltaic unit reduces the power burden on the energy storage unit, decreasing the energy storage unit's output. At t_5 = 2.5 s and t_6 = 3 s, the load unit adds loads of 1.25 kW, respectively. During the loading process, the DC bus voltage further decreases. At t_7 = 4 s, the load unit reduces the load by 2.5 kW. At t_8 = 5 s, the photovoltaic unit output power increases

with rising light intensity, reaching peak values for both light intensity and photovoltaic output power at t_9 = 5.5 s. During the gradual increase in light intensity, the DC bus voltage also gradually recovers. At 5.115 s, the DC bus voltage enters the ±2% range, the grid-connected unit inverter resumes DC bus voltage control, and the energy storage unit transitions from discharging back to charging. The battery SOC begins to rise, and the grid-connected unit inverter's power flow direction changes, beginning to supply power to the grid. At t_{10} = 6 s and t_{11} = 7 s, the load unit gradually reduces the load (Figure 13). By t_{11} = 7 s, the load unit switches to no load. At this time, the system's power units consist only of the grid-connected unit, energy storage unit, and photovoltaic unit. Due to high photovoltaic output, the energy storage unit charges the battery at full power while surplus power is fed to the grid through the inverter.

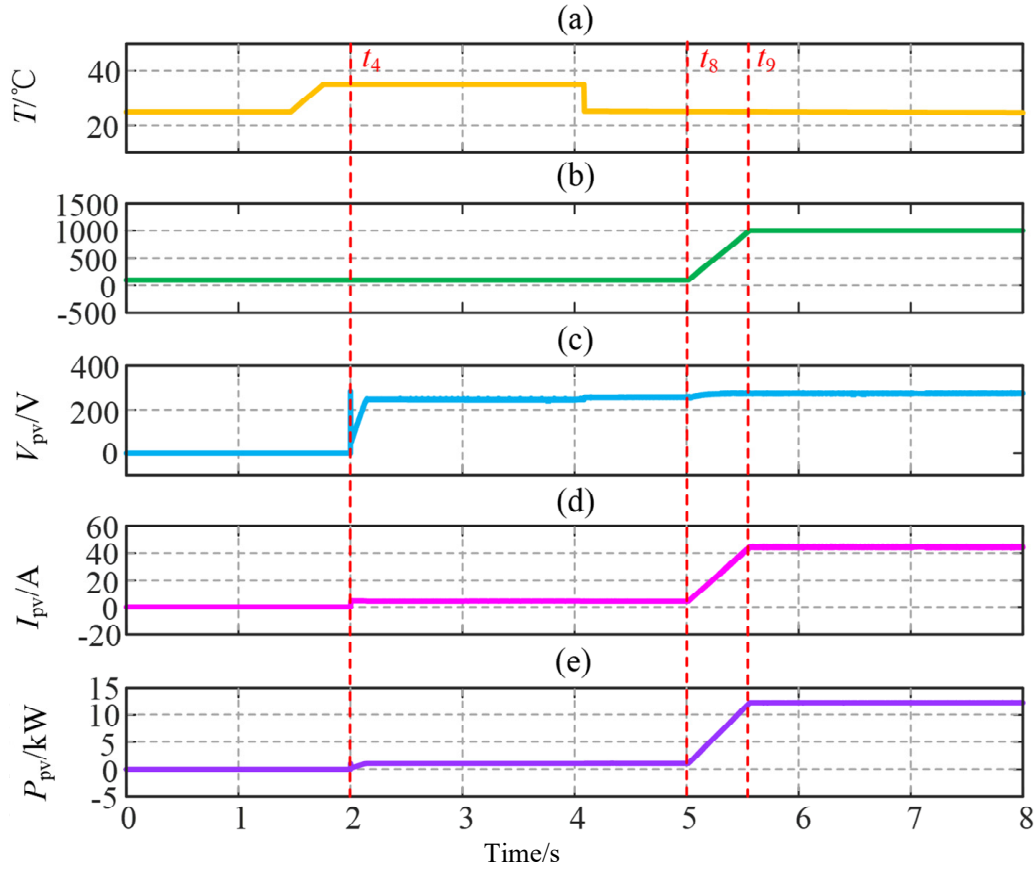


Figure 13. Current-limited grid-connected mode photovoltaic unit output waveforms: (**a**) ambient temperature; (**b**) light intensity; (**c**) photovoltaic voltage; (**d**) photovoltaic current; (**e**) photovoltaic power.

Under droop control, (Figure 14) the grid-connected unit inverter and energy storage unit converter can achieve seamless switching, maintaining the DC bus voltage in a relatively stable state without significant mutations. When the bus voltage variation is within $0.02 < |\Delta U_{dc}| < 0.05$, the energy storage unit can smoothly transition from charging or standby mode to voltage source mode by controlling the DC bus voltage. During the switching process, work mode conversion is achieved without requiring communication between the inverter and bidirectional energy storage converter.

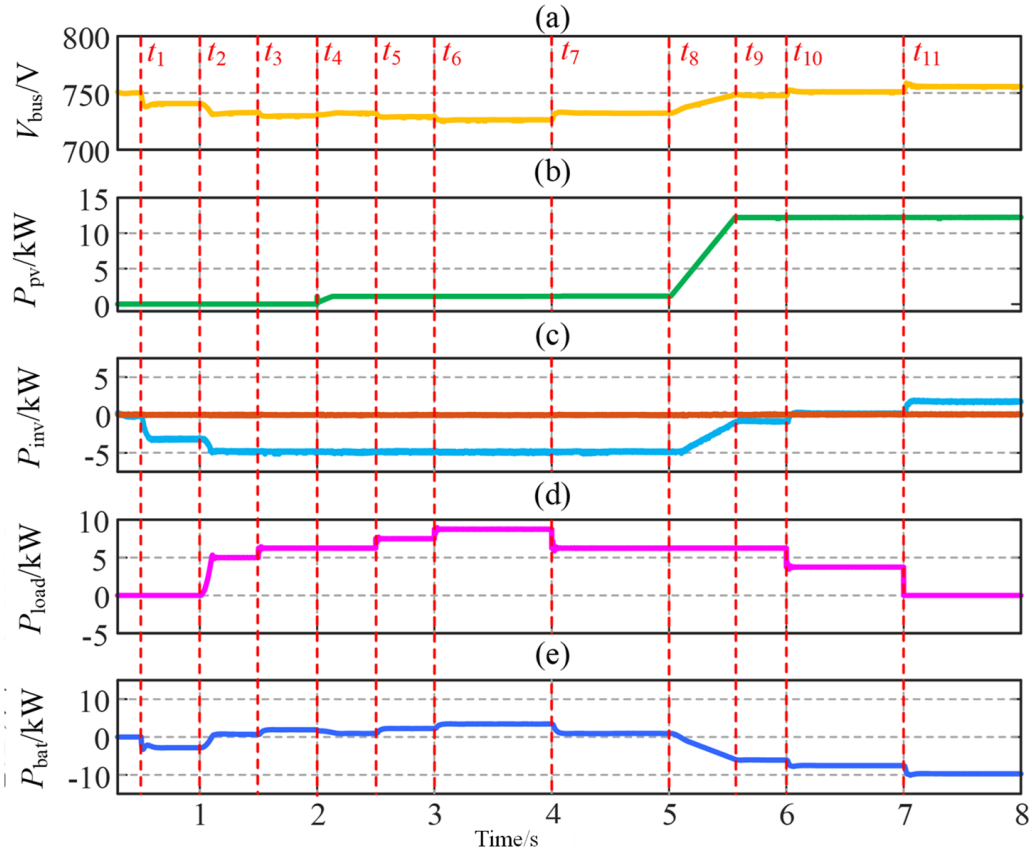


Figure 14. Current-limited grid-connected mode system dc bus and power waveforms of each unit: (**a**) system DC voltage; (**b**) photovoltaic power; (**c**) inverter power; (**d**) load power; (**e**) battery power.

4.4. Power Curtailment Operating Mode Simulation Analysis

At the start of the simulation (Figure 15), the grid-connected unit inverter establishes the DC bus voltage at 750 V (Table 4). At t_1 = 0.5 s, the energy storage unit starts with a battery SOC at 79.98%, below 80%. The bidirectional energy storage converter begins battery charging, and the battery SOC gradually increases. As shown in Figure 16a, the DC bus voltage decreases from 750 V to 742 V under droop control. At t_2 = 1 s, the DC load unit starts with a 2.5 kW load, establishing a stable 220 V DC output for the DC load power supply. Simultaneously, the photovoltaic unit initiates MPPT control, beginning to convert solar energy into electrical energy for system input. At this time, due to a weak light intensity of only 100 W/m², the photovoltaic unit power output is relatively low. At t_3 = 1.1 s, light intensity begins to rise, causing the photovoltaic output power to increase accordingly (Figure 16). At t_4 = 1.32 s, the battery charging SOC reaches 80%, causing the energy storage unit to stop operation and battery charging to cease. At t_5 = 1.4 s, the light intensity reaches maximum, and the photovoltaic unit output power also reaches its peak. During the process of increasing the photovoltaic output power, the grid-connected unit inverter's power flow direction gradually changes from absorbing power from the grid to feeding power back to the grid. Due to the high photovoltaic unit output power, the grid-connected unit inverter's grid-connected power gradually increases to the power limit value and remains constant. At this time, the power supplied by the photovoltaic unit to the DC bus exceeds the power absorbed from the DC bus by various converters, causing the bus voltage to rise, as shown in Figure 16a.

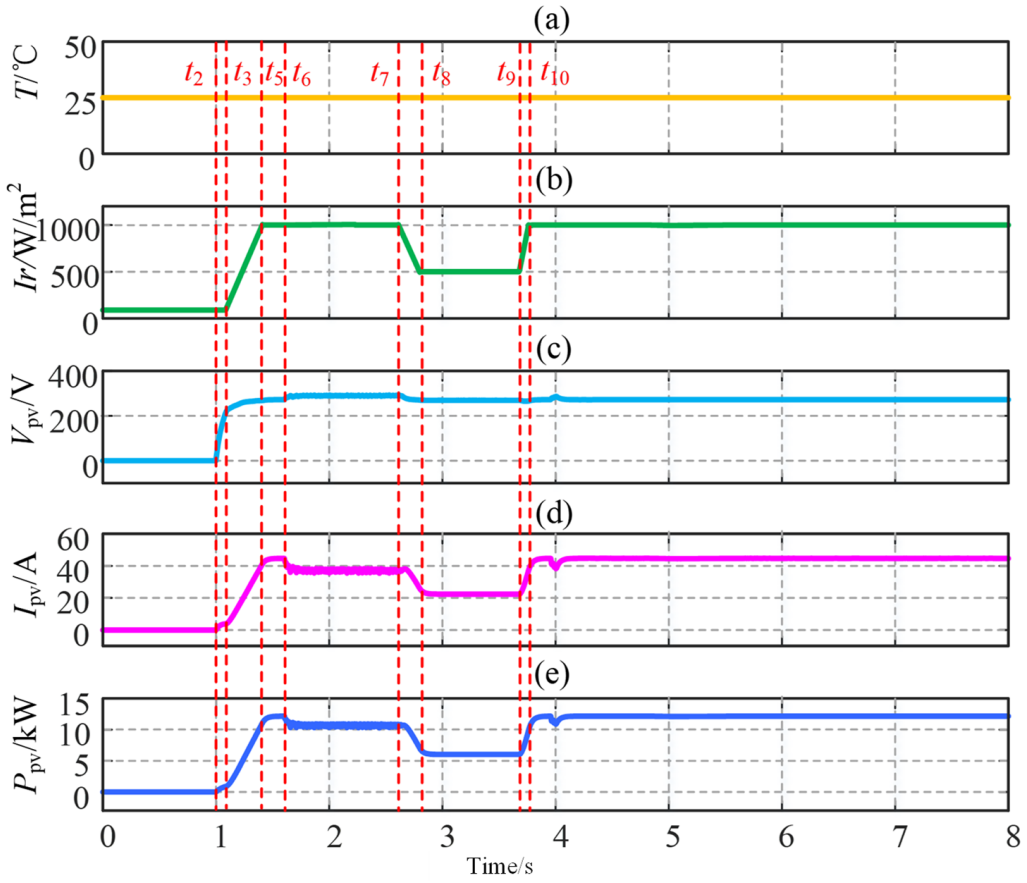


Figure 15. Photovoltaic Unit output waveforms in power curtailment operation mode: (**a**) ambient temperature; (**b**) light intensity; (**c**) photovoltaic voltage; (**d**) photovoltaic current; (**e**) photovoltaic power.

Table 4. Simulation time nodes for power curtailment operation mode.

Simulation Time T/S	Simulation Settings
0	Start simulation, grid-connected inverter establishes DC bus voltage 750 V
0.5(T1)	Energy storage unit starts, charges storage battery
1(T2)	DC load unit converter starts with 2.5 kW load
1.1(T3)	Photovoltaic unit starts MPPT control
1.4(T4)	Light intensity begins to slowly increase
2.6(T5)	Light intensity reaches maximum
2.8(T6)	Light intensity begins to slowly decrease
3.75(T7)	Light intensity reaches stability
4(T8)	Light intensity recovers
5	DC load unit loads 2.5 kW

At t_6, when the bus voltage rises to 1.075 pu, it triggers the system's power curtailment operation threshold. To ensure system safety, the photovoltaic unit needs to deviate from its original operating state, reduce the output power, and operate in constant voltage mode, controlling the system DC bus at 1.075 pu (806.25 V in this paper). The photovoltaic power curtailment operation ensures system power balance, becoming the new power balance node. At t_7 = 2.6 s, the system DC bus voltage decreases with declining photovoltaic output power and light intensity. With the energy storage unit in the saturation state, the bus voltage is controlled by the grid-connected inverter. At t_{10} = 3.75 s, the light intensity recovers, the grid-connected power returns to its maximum value of 7.5 kW, and the photovoltaic unit switches to voltage source mode operation. At t_{11} = 4 s, the load

unit adds a 2.5 kW load. At this time, the required load power and grid-connected power remain less than the photovoltaic unit's maximum output power, so the photovoltaic unit continues operating in constant voltage mode to ensure system power balance and bus voltage stability.

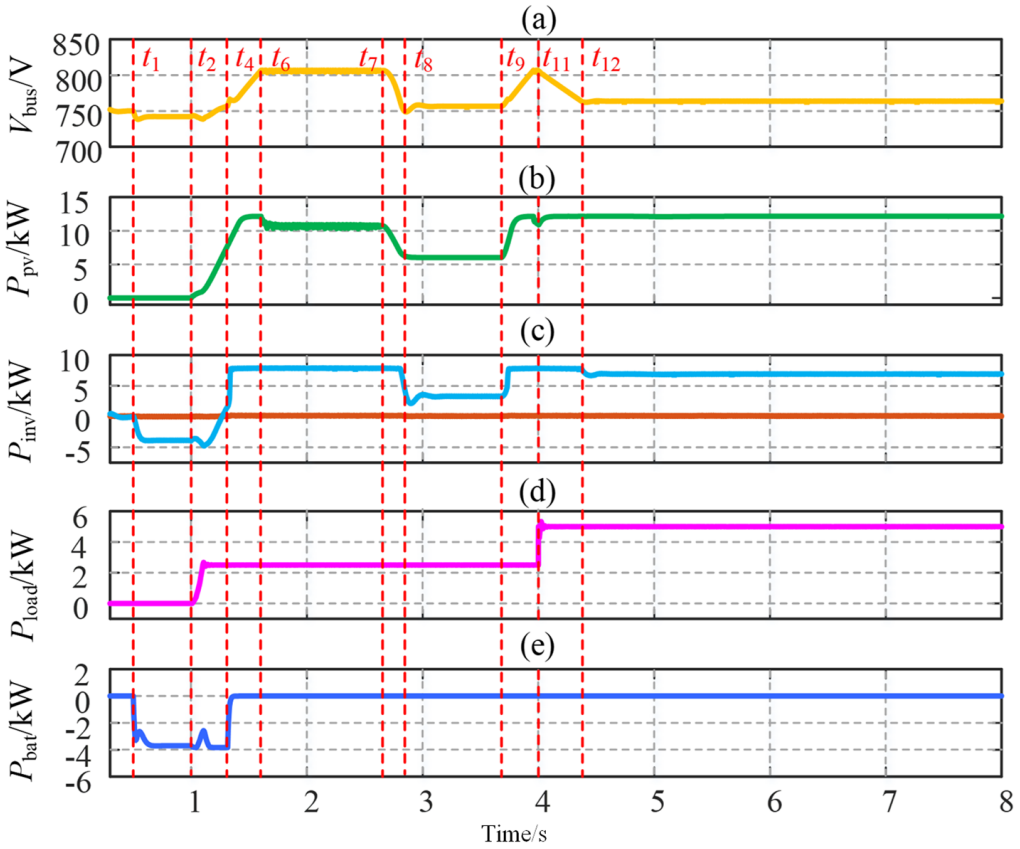


Figure 16. System DC Bus and Power Waveforms of Each Unit in Power Curtailment Operation Mode (**a**) System DC voltage (**b**) Photovoltaic power (**c**) Inverter power (**d**) Load power (**e**) Battery power.

When the photovoltaic unit output becomes excessive, it can seamlessly switch to constant voltage control mode and operate in power curtailment mode, ensuring system power balance. Additionally, when the system power demand increases or environmental conditions deteriorate, causing photovoltaic output to decrease, it can automatically switch back to MPPT mode. Seamless switching between these two modes is achievable. Throughout the simulation process, the grid-connected unit inverter and photovoltaic unit converter can change their operating states based on system DC bus voltage magnitude, ensuring stable system operation without communication requirements.

5. Experimental Verification

To verify the coordinated control strategy based on DC bus voltage proposed in this chapter, a power router was constructed as shown in Figure 17, where Figure 17a shows three DC-DC converters and other equipment, and Figure 17b shows the inverter, DC source, and photovoltaic simulator.

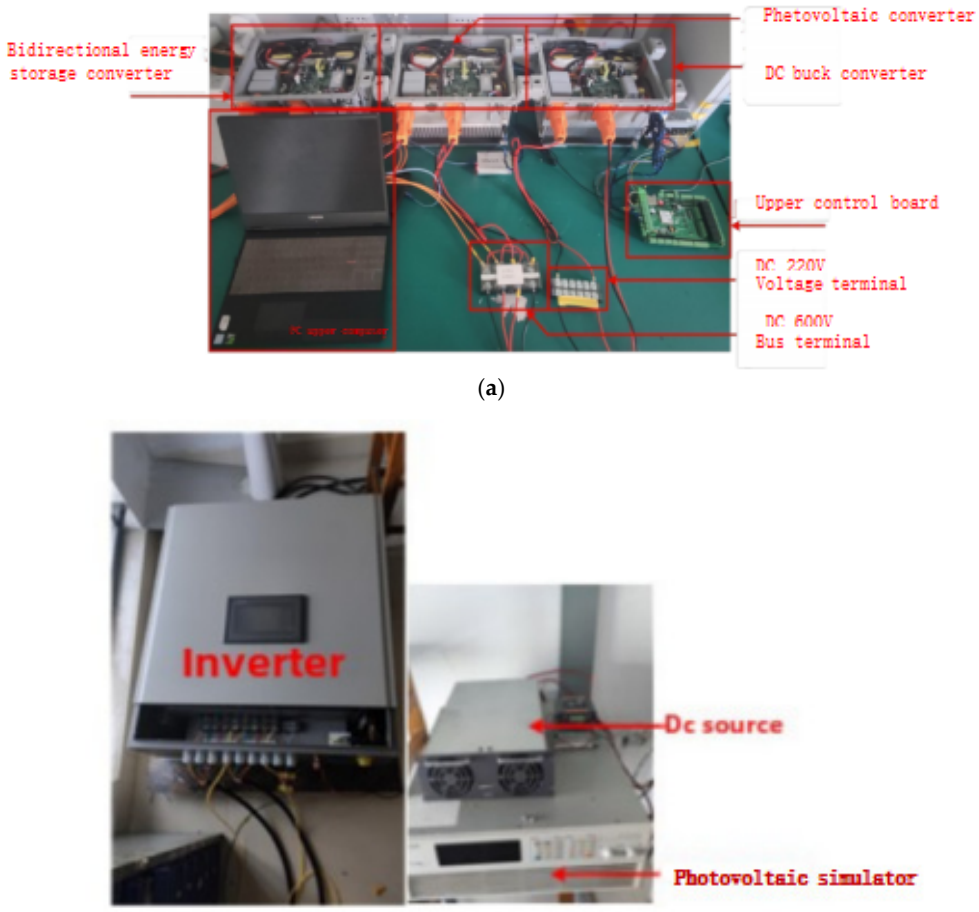


Figure 17. Physical diagram of energy router equipment. (**a**) DC-DC converters and other equipment including bidirectional energy storage converter and photovoltaic converter; (**b**) inverters and other power sources.

An operating condition experiment was conducted under energy storage-dominated control. During the experiment, a bidirectional energy storage converter was used to establish the bus voltage. Due to converter performance limitations, DC bus voltage was set to 600 V. The photovoltaic converter operated in MPPT mode, the grid-connected converter fed energy to the grid, and the load unit converter provided a stable 220 V to the DC loads. During the experiment, the photovoltaic unit's maximum power point was set to 2 kW, the grid-connected inverter's grid-connected power was set to 3.3 kW, and the DC 220 V port operated under no load.

As shown in Figure 18, the voltage waveforms during system operation include the energy storage converter's low-voltage side voltage, the DC bus voltage, the photovoltaic simulator output voltage, and the DC 220 V voltage. The figure shows that all system voltages remain stable, indicating that system power maintains balance and stability.

Figure 18 shows system current waveforms, including the energy storage converter's low-voltage side current, the inverter's DC-side voltage, the photovoltaic simulator's output current, and the DC 220 V port's output current. The voltages in each channel of Figure 18 correspond to the currents in each channel of Figure 19, representing the power at corresponding ports. Data calculations from the figures can be performed, as shown in Figure 19, proving that the system power maintains balance at this time.

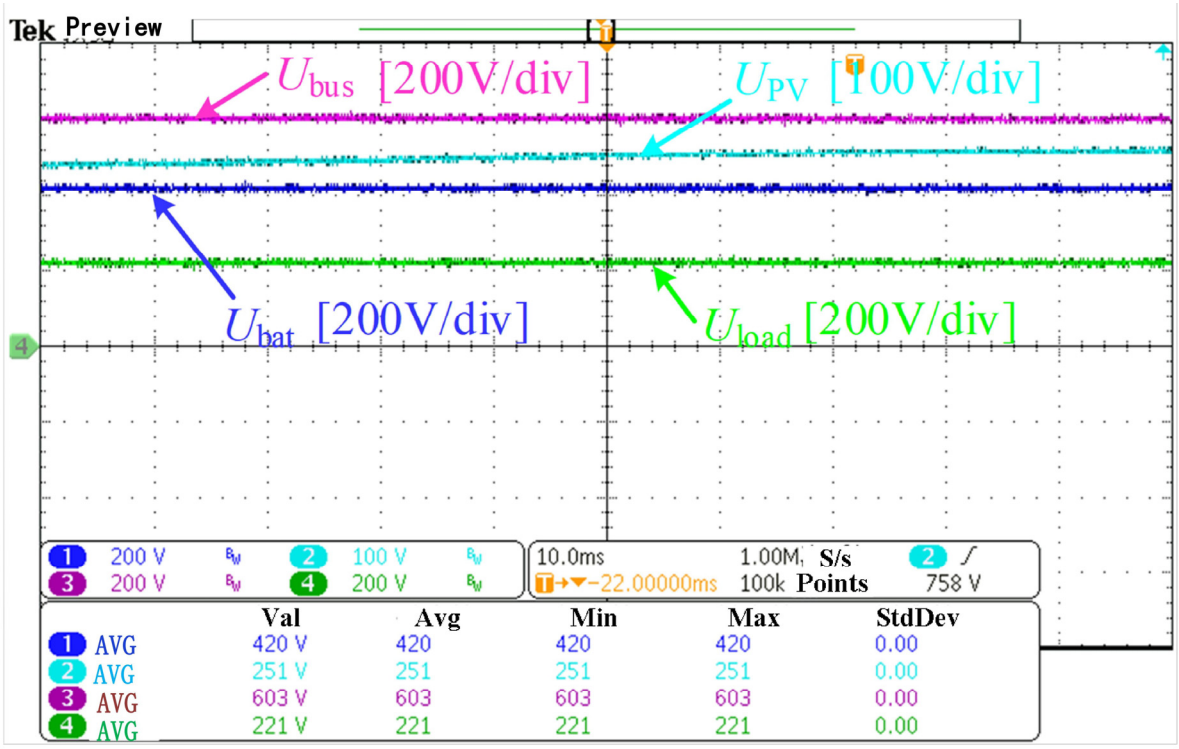


Figure 18. System voltage waveforms.

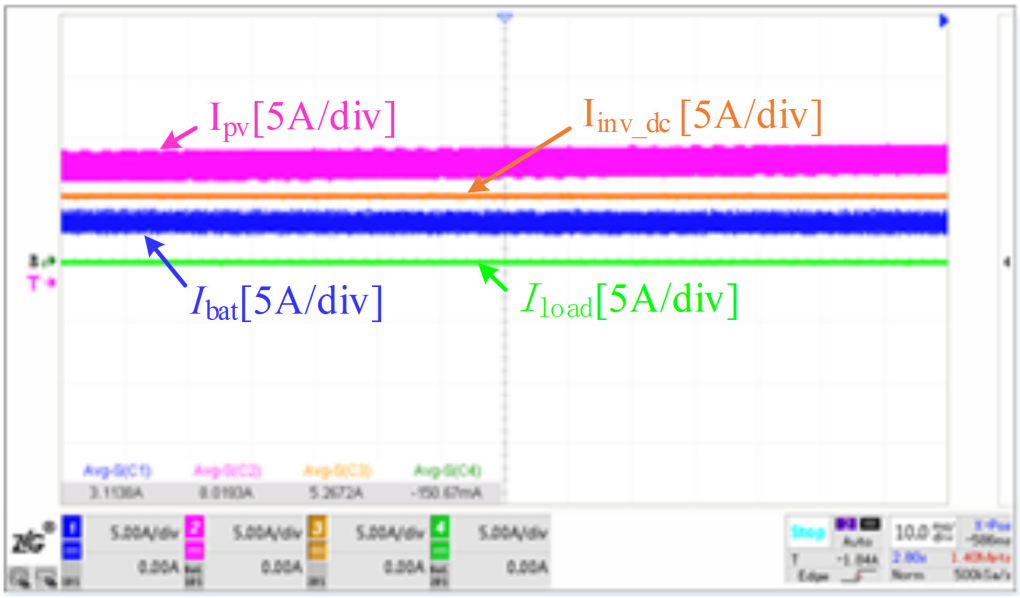


Figure 19. System current waveforms.

Table 5 shows the photovoltaic simulator parameters, and Figure 20 displays the real-time data interface of the photovoltaic simulator during system operation. The maximum power point voltage is set to 250 V with a current of 8 A, while the actual operation shows values of 251.46 V and 7.8515 A. Deviation in the voltage occurs due to the photovoltaic simulator's inherent characteristics; when different parameters are set, the simulated photovoltaic characteristics vary, affecting the output results. According to the photovoltaic simulator parameters, the photovoltaic unit is now properly tracking the maximum power point operation, inputting 2 kW of power into the system.

Table 5. Photovoltaic simulator parameters.

Parameter Name	Voc/V	Isc/A	VMP/V	IMP/A	EQ_PMP/kW	EQ_VMP/V	EQ_IMP/A
Set Value	300	12	250	8	2014.5	242.77	8.288
Actual Value	500	12	251.46	7.85	1974.3		



Figure 20. System voltage multimeter readings energy storage converter.

Figure 21 shows the voltage and current waveforms of phase C on the inverter's AC side. The system maintains sinusoidal voltage and current operation, indirectly reflecting system power stability. The inverter's voltage and current phases are identical, indicating power transfer to the AC grid.



Figure 21. Real-time data display of photovoltaic simulator.

To further verify the system's stability, Figure 22 shows voltage and current waveforms during loading of the 220 V port. Figure 23a shows waveforms when loading 494 W from no-load conditions at port 3, and Figure 23b shows waveforms when loading 988 W. The dynamic loading process demonstrates that the bus voltage remains stable with minimal fluctuation. The 220 V port shows a noticeable voltage drop when transitioning from no load to a loaded state, due to poorer voltage control performance during low-current no-load conditions compared to loaded conditions. After 220 V port voltage recovery, stable operation is maintained.

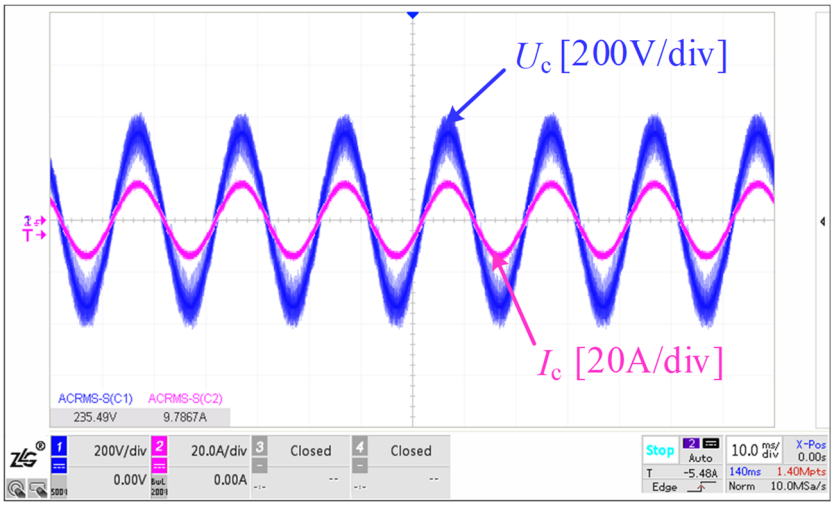


Figure 22. Phase C voltage and current waveforms on inverter AC side.

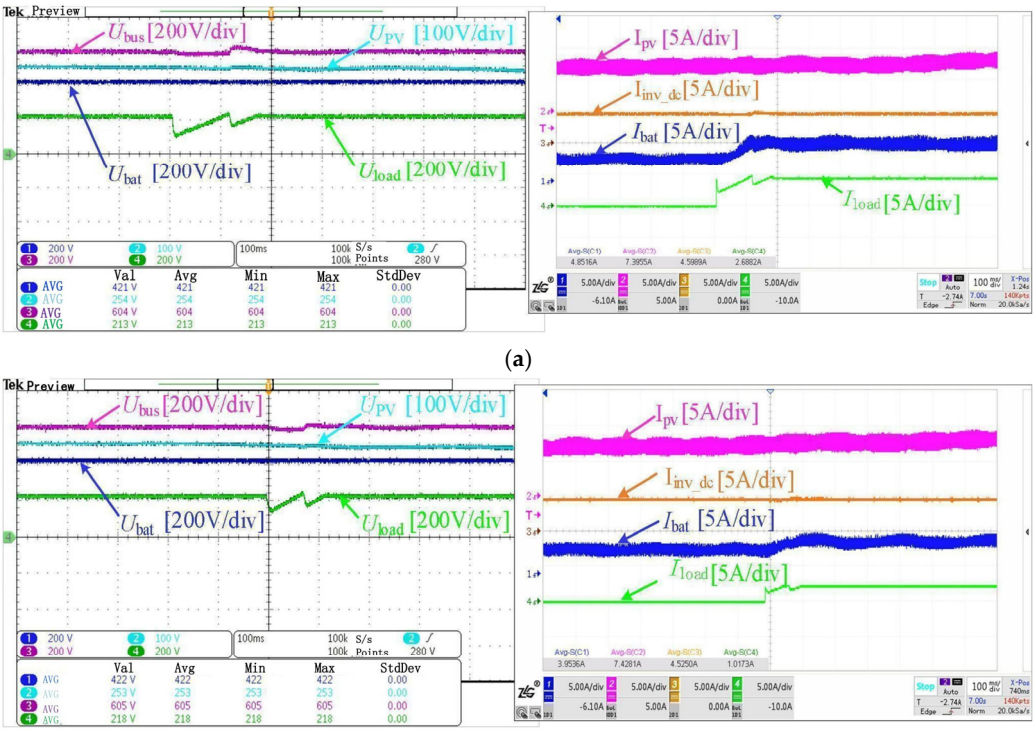


Figure 23. System dynamic voltage and current waveforms. (**a**) DC 220 V port loading 494 W. (**b**) DC 220 V port loading 988 W.

6. Conclusions

This study proposes a coordinated control strategy for multi-port power routers based on DC bus voltage droop regulation, addressing the limitations of existing methods that rely on communication and complex control units. By enabling automatic mode switching without additional communication mechanisms, the proposed strategy significantly enhances the adaptability and reliability of the system, simplifies control logic, and ensures stable operation across different modes. This innovative approach provides new insights into the practical application of power routers.

The innovations of this study are mainly reflected in the following aspects:

1. A coordinated control strategy based on DC bus voltage droop regulation is proposed, eliminating the need for additional communication mechanisms and reducing system complexity.
2. Seamless switching between different operating modes of the multi-port power router is achieved, addressing the complexity and reliability issues of existing methods during mode switching.
3. The effectiveness of the proposed strategy in residential applications is verified through experiments, providing new insights into the practical application of power routers.

Author Contributions: Software, C.Z.; Formal analysis, P.Z.; Data curation, H.W. and N.L.; Writing—original draft, P.Z. and Q.D.; Project administration, G.S. All authors have read and agreed to the published version of the manuscript.

Funding: This research received no external funding.

Data Availability Statement: The original contributions presented in this study are included in the article. Further inquiries can be directed to the corresponding author.

Conflicts of Interest: C.Z., G.S., H.W., N.L. and Q.D. were employed by China Electric Power Research Institute Co., Ltd. The remaining authors declare that the research was conducted in the absence of any commercial or financial relationships that could be construed as a potential conflict of interest.

References

1. Zhao, Z.; Feng, G.; Yuan, L.; Zhang, C. The development and key technologies of electric energy router. *Proc. CSEE* **2017**, *37*, 3823–3834.
2. Ge, Q.C.; Yao, G.; Zhou, L.D. Research Status and Prospects of Electric Energy Router Technology. *Electr. Power Constr.* **2019**, *40*, 105–113.
3. Wang, R. *Research on Key Technologies of Power/Data Integrated Energy Router*; Zhejiang University: Hangzhou, China, 2019.
4. Gadelha, V.; Sumper, A.; Bullich-Massagué, E.; Aragüés-Peñalba, M. Electrical grids based on power routers: Definition, architecture and modeling. *IEEE Access* **2023**, *11*, 10004–10017. [CrossRef]
5. Zhang, S.; Ji, Y.; Wang, Q.; Yao, W. Three-layer optimization control strategy of energy Router in household DC microgrid. In Proceedings of the 2020 IEEE 9th International Power Electronics and Motion Control Conference (IPEMC2020-ECCE Asia), Nanjing, China, 29 November–2 December 2020; pp. 693–698.
6. Li, D.; Sun, Q.; Wang, R.; Sui, Z. Transient Stability Analysis and Enhancement of Inverter-Based Microgrid Considering Current Limitation. *IEEE Trans. Power Electron.* **2024**, *40*, 2429–2441. [CrossRef]
7. Ertekin, D. A High Gain Switched-inductor-capacitor DC-DC Boost Converter for Photovoltaic-based Micro-grid Applications. *CSEE J. Power Energy Syst.* **2023**, *34*, 2398–2410. [CrossRef]
8. Zhu, J. *Research on Coordinated Control Strategy of DC Microgrid with PV and Storage Ststem*; Harbin Institute of Technology: Harbin, China, 2020.
9. Zhang, J.; Zhao, R.; Gao, L.; Ji, W.; Yang, P.; Wu, Z. DC Bus Voltage Stability Control Strategy for DC Microgrid. *Power Syst. Technol.* **2021**, *45*, 4922–4929.
10. Feng, G.; Zhao, Z.; Yuan, L. Synthetical Control Technology of Electric Energy Router Based on Energy Balance Relationship. *Trans. China Electrotech. Soc.* **2017**, *32*, 34–44.
11. Tu, C.; Luan, S.; Xiao, F. A Coordinated Power Control Strategy of Three-port DC Energy Router Based on Droop Phase-shift. *Power Syst. Technol.* **2019**, *43*, 4105–4114.
12. Nie, Z.Q. *Research on Grid-Connected/Islanding Seamless Transfer of Photovoltaic Energy Storage System*; Beijing Jiaotong University: Beijing, China, 2016.
13. Xia, J. *Study and Comparison of Three-Phase Grid-Connected Inverter with Droop and VSG Control Methods*; Zhejiang University: Hangzhou, China, 2020.
14. Sun, D. *Research on MPPT Control for Photovoltaic Power System*; Shandong University: Jinan, China, 2014.
15. Zhang, C.; Zhao, Z.; Sang, H. Review of photovoltaic cells modelling. *Power Technol.* **2016**, *40*, 4.

16. Cai, S. *Research on the Inverter and MPPT Algorithm of Grid-Connected PV System*; China University of Mining & Technology: Beijing, China, 2017.
17. *GB/T 40097-2021*; Functional Specifications and Technical Requirements of Energy Router. China Electricity Council: Beijing, China, 2021.

Disclaimer/Publisher's Note: The statements, opinions and data contained in all publications are solely those of the individual author(s) and contributor(s) and not of MDPI and/or the editor(s). MDPI and/or the editor(s) disclaim responsibility for any injury to people or property resulting from any ideas, methods, instructions or products referred to in the content.